Development of a low voltage railgun in the context of a swept lightning stroke on an aircraft

Vincent Andraud, Rafael Sousa Martins, Clément Zaepffel, Romaric Landfried, Philippe Teste

Development of a low voltage railgun in the context of a swept lightning stroke on an aircraft

V Andraud[1], R Sousa Martins[1], C Zaepffel[1], R Landfried[2] and P Testé[2]

[1]DPHY, ONERA, Université Paris Saclay, F-91123 Palaiseau, France
[2]Laboratoire GeePs, CNRS UMR8507, Université Paris Saclay, CentraleSupélec, 91190 Gif-sur-Yvette, France

E-mail: rafael.sousa_martins@onera.fr

ABSTRACT

When aircraft are struck by lightning, the aircraft's structural fuselage and components are stressed by electrical and thermo-mechanical constraints, which imposes a need for reliable experimental test benches to design accurate and enhanced lightning protection. In order to reproduce the in-flight conditions of an aircraft in a laboratory, the aim of this work is to design and implement launch equipment able to propel aeronautical test samples at speeds characteristic of an aircraft – from 10 m/s for ultra-light gliders to 100 m/s for airliners – before striking it with an electric arc within the laboratory dimensions of several meters. After a comparison of several propulsion techniques, the selected solution is an augmented electromagnetic railgun launcher. Since it requires the injection of a high current to be efficient and a low voltage operative point for safety considerations, specific and original electric generator and rail structures have been designed and experimentally implemented. Particular attention has been paid to the experimental problems encountered and mainly the sliding contact, since almost no literature references are available for railgun equipment at this level of performance. Then, based on different experimental implementations, a dynamic and ballistic model of the projectile has been developed to evaluate and characterize friction forces with the aim of predicting launcher performances with different inputs. This serves to control the speed of the material test sample during the lightning strike. Finally, the railgun equipment has been coupled to a lightning generator to reproduce the lightning strike of an aircraft respecting in-flight conditions.

I. INTRODUCTION

In the aeronautical industry, the risk of lightning strike is taken into account from the very design of aircraft since the phenomenon statistically occurs every 1000 to 10,000 flight hours. Since this phenomenon involves a lightning channel that is static in the terrestrial reference frame and an aircraft that can reach a speed of 100 m/s in the take-off or in the landing phase, there is a displacement of the impact area – the arc root - on the outer skin of the aircraft. This phenomenon is referred to as the s*wept-stroke* phenomenon. Depending on the material and the geometry of the fuselage and the speed of the aircraft, this displacement varies in nature. Indeed, it can take the aspect of a continuous sweeping in the outer-skin or can consist in successive reattachment spots. This latter type of displacement is particularly observed with the presence of rivets, fasteners, or seams.[1] Thus, all the parts of the aircraft are exposed to the risk of direct electrical and thermomechanical damage induced by lightning strikes. Therefore, it is necessary to understand the physical mechanisms that drive the displacement of the arc root in order to optimize lightning strike protection. A significant bibliography exists on the modelling of this displacement combining electromagnetism and fluid mechanics

equations.[2-4] However, existing simulation codes have still not been validated by the implementation of an experimental aircraft simulation that could be struck by lightning to create a reference database for the physical parameters of the phenomenon.

In order to conduct a representative experiment involving a lightning strike to an aircraft, a means for propelling an aeronautical test material to the speed of an aircraft during take-off or landing – that is to say from 10 m/s for ultra-light gliders to 100 m/s for airliners – has to be found. Since this experiment has to be conducted indoors to enable the use of fine optical diagnostics, there is a limit to the available space. If a limit of 5 m is set, the propulsion technology has to produce a mean acceleration of several hundred g-forces to propel the test equipment to the given speeds. Aluminum plates with a thickness of between 0.4 and 1 mm and length and width dimensions of several tens of cm were considered for the test equipment, resulting in sample masses varying from 100 to 500g. Thus, the mean force applied by the propulsion on the equipment has to reach 500 N.

A. Other published means of propulsion for studying the swept-stroke phenomenon

Few references for other means of propulsion implemented for the study of the swept-stroke phenomenon are available in the literature. Some experiments consist in placing the arc in motion instead of the test equipment since it can reach rapid speeds with self-induced[5,6] or external magnetic field[7] means or wind tunnel means[8,9] but have the disadvantage of being less representative of the phenomenon since the lightning arc column is artificially displaced and so cooled down by the stationary air[1]. In addition, the arc is swept along both electrodes and so its movement is affected by its interactions both with the anode and the cathode. In reality, the lightning channel is stationary in air and only the part that is situated in the vicinity of the test equipment surface is subjected to relative velocities.[3,4]

More representative experiments place the test equipment in motion relative to a static electric arc. Different means of propulsion are available in the literature, such as placing the test equipment on the top of a truck[1], using the release of a stretched elastic band[1] or using chemical propulsion[10]. In these three experiments, the speeds reached were respectively 15 m/s, 20 m/s and 72 m/s. The latter speed is of the same order of magnitude as the physical phenomenon, but the use of a chemical propellant represents safety issues if it is conducted in an indoor laboratory. Thus, this option was rejected since the use of fine optical and electrical diagnostics to capture the phenomenon are easier to implement within the infrastructures of an indoor laboratory.

B. Selection of a relevant means of propulsion

Other means of propulsion have been investigated, including mechanical, fluid, chemical and electromagnetic release of energy to transfer sufficient propulsion to the aeronautical equipment in order to reach the desired velocity.

Considering the release of a stretched or compressed solid to provide propulsion, the speed of release is limited by the speed of sound propagation. In plastic and rubber-like materials, stretched elastic cannot release at a speed faster than 40 m/s.[11] In metals, this speed reaches more than a few thousand m/s[12] but the maximum relative longitudinal elongation is at the most 0.1 % to be still able to consider Hooke's law[13] so that transmitting propulsion to an aircraft equipment is not possible. Moreover, the speed of wave propagation in a metal spring is around 10 to 20 m/s[14], which is not sufficient for our

application. Finally, a flywheel is capable of attaining a maximum peripheral speed of some several hundred m/s before exceeding the limit of elastic behavior.[15] However, the costs, the encumbrance and the bulk of the infrastructure are prohibitive.

Acceleration can also be achieved by expelling a body – liquid or gas – very quickly according to the conservation of impulsion principle. The speed of the released body is improved by reaching high pressure levels. For instance, propulsion by means of hot water has been used to accelerate sleds from 23 m/s^2 to a maximum velocity of 225 m/s.[16] Apart from the limited acceleration that can be obtained, using water propulsion indoors without a structure to ensure the protection of electronic devices and with coupling to an electric arc are additional drawbacks. The same problem occurs with a gas propulsion application such as that of Dobbing and Hanson.[10] Nevertheless, it is possible to propel a test sample using gas propulsion by increasing the pressure in a gas chamber – compressing a gas to high pressure or releasing it by a chemical reaction. This equipment is referred to as a gas gun in the literature and is mainly used as launcher technology for impact testing in laboratories: as an example, the laboratory STAR of Sandia (NISA) has a two-stage light gas gun that can propel a projectile of several dozens of grams up to 7.5 km/s, using a pressure of 650 GPa.[17] However, this technology requires specific infrastructures to control the pressure in the gas chamber, which makes this option difficult to implement.

Propulsion means using electromagnetic forces in systems with high transient currents, magnets or coils is a common way of reaching high velocities and high accelerations. Cassat et al.[18] describe the different performances of such a system in industry. Depending on the accuracy, the payload and the speed performance, these different technologies – both using an electromagnetic phenomenon – are more or less relevant for our application. Indeed, maglevs, catapults, rollercoasters, conveyors, machine tools, robotics, precision manufacturing and small stroke machines are not designed to reach, at the same time, acceleration levels more than several g and speed levels for more than a dozen m/s, but are rather useful in precision positioning applications, which is not a main concern for our problem. Thus, the remaining possibilities are electromagnetic launcher technologies: mainly railgun and coilgun facilities. Since coilgun technologies require a highly accurate synchronization in supplying power to the coils, only the railgun option has been investigated in this paper.

C. Brief theory and paradigm

Railguns have been studied and developed as very high-speed launchers for various applications ranging from military developments, the launch of commercial and military aircraft, the launch of micro-satellites into space and impact-fusion implemented by acceleration of fusible material.[19-23] It consists in injecting a high current into a sliding armature inserted between two rails. This high current generates a strong magnetic field that interacts with the current that forms it to provide a Laplace force that applies on the sliding armature and thus provokes its propulsion, as shown in Fig. 1. Speeds reaching up to 10 km/s are reported[23] for projectiles of several grams, whereas the ISL institute has reached a speed of 2.3 km/s for a load of 0.6 kg using a current of 2 MA in the railgun circuit.[24]

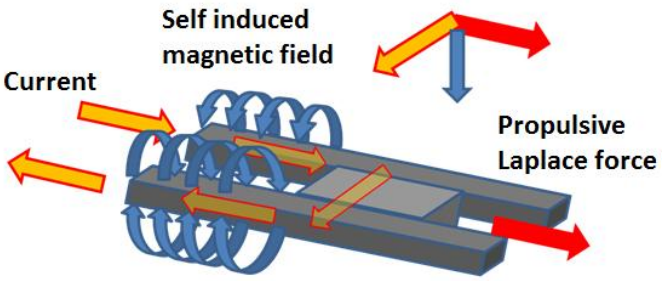

FIG. 1. Diagram of the principle of a railgun.

To calculate the current level that is required for our application, assuming the desired force is 500 N, the standard equation in the literature is used:[25]

$$F = \frac{1}{2} L' I^2 \tag{1}$$

where *F* is the force provided to the sliding armature, *L'* is the inductance gradient of the railgun and I is the current. *L'* only depends on the rail geometry and is assumed to be constant over time for a geometry consisting of two parallel rails. Its value in the literature varies between several tenths to one µH/m. Thus, it means the level of current is in the range of 30 kA if the parameter L' is set at 1 µH/m. However, since the current must be provided for a few meters and the desired speed is several 10 m/s, a good electrical sliding contact must be ensured for several tenths of ms, which is unusual for conventional railguns where the maximum sliding contact duration is some several ms.

The main objectives of this paper are to present the design and the performances of a low voltage railgun developed in the aeronautical context of lightning strikes to aircraft. Section I introduces the required performances in terms of speed and acceleration in order to be representative of the phenomenon and explains the selection of railgun technology. Section II aims to present and describe the electrical circuit and the geometry of the developed railgun. Section III discusses the new technical and practical issues raised by this unconventional low-voltage railgun with long duration sliding contacts. In section IV, the performances achieved by the railgun are presented and compared to a model. In section V, the coupling of the railgun with a sweeping arc is implemented.

Usually, in railgun terminology, the projectile is composed of the dead mass or sabot which ensures electrical circuit closure and consequently the transmission of the electrical energy of the circuit to the kinetic energy to the projectile through Laplace force, and the payload that is used for the railgun application. In our case the payload is a test material used to study the gliding arc phenomenon. However, since sections II, III and IV are devoted to the study of experimental railgun issues and performances, the focus is not on the payload since the latter does not play a role in the railgun study. Thus, sections II, III and IV only consider the application with the sabot and the use of the payload is developed in section V.

II. DESIGN OF THE LOW-VOLTAGE ELECTRICAL CIRCUIT, GEOMETRY AND EXPERIMENTAL SET-UP

A. Paradigm of low voltage railgun

Most electric railgun systems require a bank of capacitors capable of storing several MJ and of delivering power levels up to several GW and currents up to 2 MA.[24] Thus, the standard capacitors used for this application have an operating voltage of from several tens of kV to several hundreds of kV but with a capacitance equal to or less than several mF.[25] Thus, the peak level of current cannot be maintained for more than several hundreds of µs, even with several current distributions all along the rail using several capacitor banks.[26] In our application, the speed of 100 m/s for several hundreds of grams could be reached in hundreds of µs with a current over several hundred kA. However, this would require a very high-power capacitor bank. Moreover, since the railgun has to be coupled with an electric arc provided by an electric generator charged up to 2 kV, it is interesting to work with the minimum voltage level possible for safety and practical reasons.

The objective is to achieve a mean current injection that does not exceed 30 kA in order to design a current generator with the minimum of energy possible that could provide the required propulsion. Considering a mean force of 500 N is required all along the entire rail length – several meters - to obtain a constant acceleration of 1000 m/s^2, the current injection time has to be around 100 ms. As in an RC discharge injection circuit, the electric time constant τ has to be over 10 times the application time to guarantee a decrease in current level below 10%, so the electrical time RC is set at 1s. The typical value of R in railguns is between 1 mΩ and 10 mΩ. Thus, the capacitance of the capacitor bank has to be above 1000 F.

Since new capacitor technology – referred to as ultra-capacitors – with high capacitances and low voltages has been available for several years[27], this range of values can be achieved in a compact volume. The models employed in this experiment are Maxwell Technology 3000 F capacitors, part number BCAP3000P and Eaton technology 3000 F capacitors, part number XL60-2R7308W-R and have already been used for a low voltage railgun application in the work of Starr and Youngquist.[28] Indeed, they used 24 of these capacitors to provide 4 kA to a 300 g sabot that reached an acceleration of 120 m/s^2 and a speed of 13 m/s after 1 m of rail. The main drawback of this technology is the low maximum operating voltage of the component, 2.7 V. To deliver the required 30 kA, a capacitor bank of 12 × 12 capacitors of the aforementioned models was used. The maximum operating voltage is thus 32 V. The maximum allowable peak current is 1900 A for the Maxwell model and 2400 A for the Eaton model, therefore a maximum current of 24,000 A was employed to avoid degradation.

B. Electrical design

A maximum voltage of 30 V makes it possible to provide a current of 24 kA only if the total resistance of the circuit is close to 1 mΩ. Therefore, the electrical components, the geometry and the materials of the rails have to be selected with care. A diagram of the electrical circuit is given in Fig. 2. The resistive elements of the circuits are the capacitor bank, the switch component – that is necessary to trigger the current injection, the connecting wires, the rail itself and the electrical contact between the sabot and the rail as well as the contact losses in general. Figure 2(a) represents a diagram of the railgun electrical circuit and Fig. 2(b) represents the railgun equivalent electrical circuit in terms of electrical components.

(a)

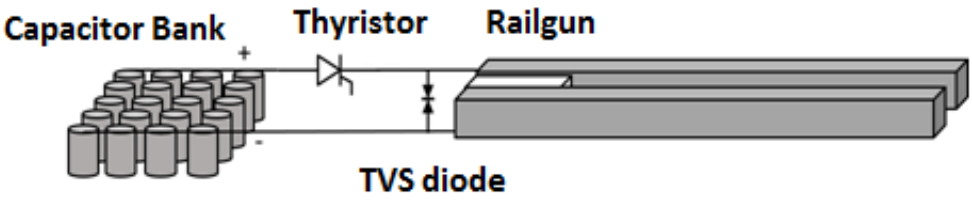

(b)

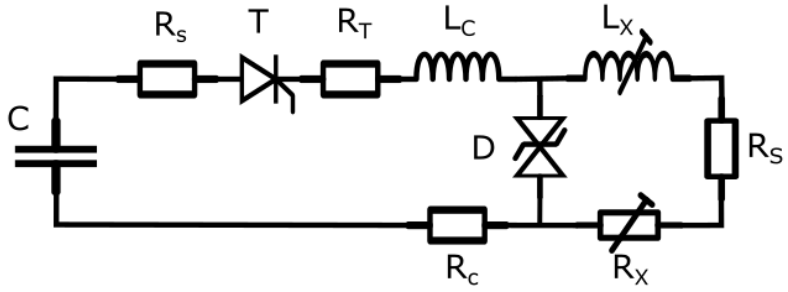

FIG. 2. Electrical diagram (a) and equivalent electrical circuit (b) of the railgun.

The capacitor bank is represented with an equivalent capacitor C of 3000F. The capacitor model has an equivalent series resistance of 0.23 mΩ and a bank of 12 series layers of 12 parallel capacitors is used, the equivalent total resistance R_S is 0.23 mΩ. For the switch component, a thyristor DCR7610H28 model is selected because it is able to withstand a continuous current of 30 kA with an equivalent resistance of 52 μΩ, but causes a voltage drop of 1 V. Three of these components are assembled in parallel to lower the equivalent resistance to 17 μΩ and decrease the stress on each component while keeping a similar voltage drop of 1 V. They are represented by the thyristor T and the resistance R_T in the equivalent circuit. The conductive wires are bars of copper adding 0.45 mΩ resistance mainly due to the supplementary losses of threaded contacts and are represented by a resistance R_C in the electrical circuit. The inductance L_C represents the addition of the internal inductance of the bank of capacitors, the internal inductance of the thyristors and the inductance of the conductors. It is measured with an RLC-meter (Stanford Research Systems SR-720) at a frequency of 100 kHz and has a value of 1.8 μH. The importance of the TVS diode will be tackled in Sec. III.D. The rails consist of two bars of copper with a section of 12 × 22 mm^2 and 2 meters length. Thus, the resistance R_X of the rails varies from zero to 0.26 mΩ when the sabot reaches the end of the track. As will be discussed in Section III, the resistance R_S composed of the contact resistance between the sabot and the circuit and the sabot resistance itself can be neglected. Thus, the total resistance of the circuit is about 1 mΩ at the beginning of the movement and reaches 1.25 mΩ at its end. Considering a constant voltage in the capacitor bank, this resistance surge during sabot movement will induce a loss of 25 % on the injected current at the end of the rail affecting the acceleration accordingly. L_X represents the variable inductance of the rails and is evaluated in Sec. II.C.

C. Mechanical design

Since the passage of the sabot between the rails can cause damage due to and bad electrical contact, replaceable aluminum angles are screwed onto the copper bars and ensure electrical contact with the sabot. These angles are 2 mm thick and can be easily changed when they turn out to be too damaged after several shots of the railgun. Two PTFE bands, 1 mm thick, are screwed below and above the rail to encapsulate the sabot and reduce friction with the sabot body. 2 mm thick aluminum bands are screwed above the PTFE bands to provide the sabot with more rigidity. All of these elements are screwed together in a bulk TIVAR plane. The distance between the two rails is 50 mm. An image of the assembly of the rails is shown in Fig. 3 and a front view is shown in Fig. 4. In Fig. 3, black electrical tape is added at the end of the rails in order to avoid electric discharge on the rails coming from the lightning generator that will be coupled with the facility, forming an electric arc at the muzzle of the rails.

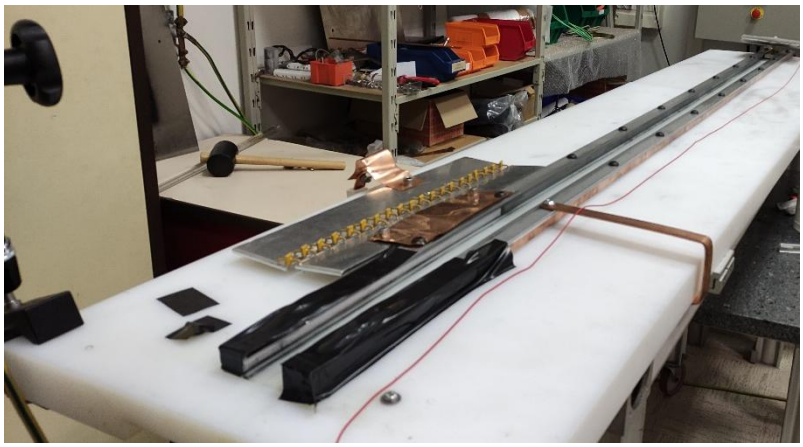

FIG.3. Assembly of the rails.

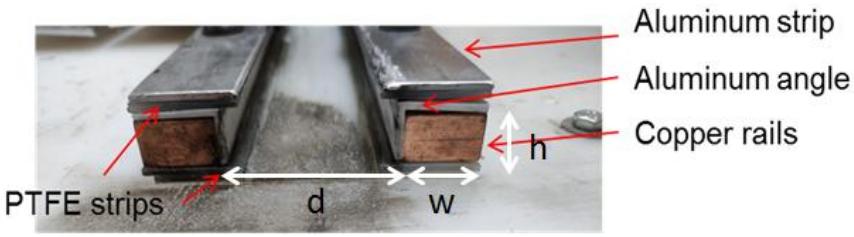

FIG. 4. Front view of the rails highlighting the different parts of the mechanical setup.

From these geometrical parameters, an estimation of the inductance gradient is given in the formula for parallel rectangular conductors that is valid for the DC case[29]:

$$L' = \frac{\mu_0}{\pi}\left(ln\left(\frac{d+w}{w+h}\right) + \frac{3}{2} + \Delta_k - \Delta_e\right) \tag{2}$$

where L' is the inductance gradient, μ_0 is the vacuum permeability, d is the distance between the rails, w is the width of the rails and h is the height of the rails in respect with Fig. 4. Δ_k and Δ_e are defined in tables[29] and depend on the d, w and h geometrical parameters. For our geometry, these latter two terms are negligible. Thus, the calculation with d, w and h being respectively equal to 50, 22 and 12 mm gives a L' of 0.9 µH/m, which is close to the desired 1 µH/m. Also, measurements were performed with an RLC-meter (Stanford Research Systems SR-720) at a frequency of 100 kHz to check this value. A linear inductance of 0.82 µH/m was found. A picture of the final set-up is shown in Fig. 5.

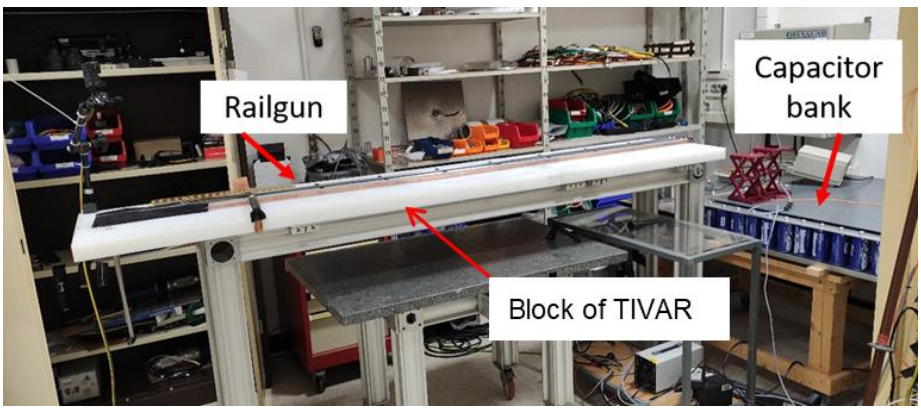

FIG. 5. Picture of the complete electrical and mechanical set-up of the railgun. The capacitor bank is composed of 12 × 12 ultra-capacitors.

NdFeB magnets were added to the structure to give an extra magnetic field that interacts with the current injected into the railgun and increases the Laplace force. This addition of permanent magnets in a railgun facility is often referred to as augmented railgun.[30] Eleven magnets of 150 mm length, 30 mm width and 30 mm height were inserted into the block of TIVAR all along the railgun tracks and covered by a 2 mm thick PTFE strip. They are thus separated by 3 mm from the sabot with the additional 1 mm strips of PTFE under the copper bars that encapsulate the sabot. Figure 6 shows a truncated side-view of the rails illustrating the insertion of the permanent magnets into the block of TIVAR under the rails.

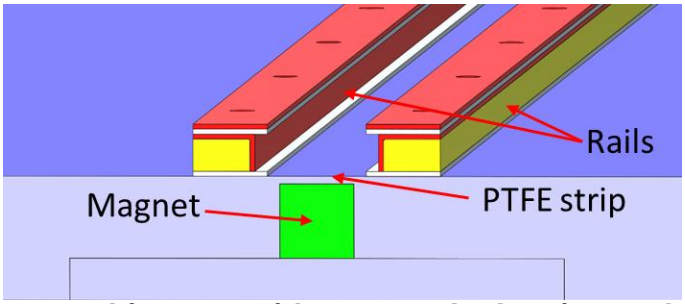

FIG. 6. Truncated front-view of the augmented railgun from a schematic.

The magnetic field imposed by the magnets at this distance is measured using a gaussmeter and have a value of around 300 mT at 3 mm from the rails at the center of the magnet. Thus, the extra-force provided by the magnets is given by the formula:

$$F = BwI \tag{3}$$

where F is the Laplace force, B is the magnetic field at the position of the projectile, w is the magnet width and I is the current in the rail. If the current is equal to 24 kA, the extra force has a value of 220 N.

D. Set-up measurements

Current measurements were carried out using a PEM CWT AC CWT60LF probe. Voltage measurements were carried out using Lecroy PPE5KV voltage probes. A high-speed camera (HSC) was used to evaluate the sabot position and speed. The HSC was a Phantom V711 from Vision Research (CMOS sensor of 1280 × 800 pixels of 20 μm^2) and was set to work with a sampling rate around 20 kfps (kilo frames per second).

III. MAIN EXPERIMENTAL ISSUES

For sections III and IV, except for the subsection III.A, the graphs presented to discuss the experimental issues and the experimental results refer to shots whose characteristics are given in Table I. This table numbers the exploited shots so that they can be referred to more easily for the discussions.

TABLE I. Numbering and characteristics of the different shots analyzed.

Shot n°	Mass (g)	Current peak (kA)	Initial Voltage (V)	Lubricant	TVS Diodes	Muzzle velocity (m/s)
1	79.6	22.5	24	yes	yes	90
2	93.2	22.5	24	no	no	68
3	101.7	22.9	24	yes	no	77
4	186.2	23	24	yes	yes	60

A. Contact transition

The main practical difficulty in implementing a railgun is to maintain the current injection while the sabot is moving. A good electrical contact has to be ensured when the sabot is subject to high acceleration to avoid the formation of a gap between the conductors and the rails. Any gap would form an electric arc to maintain the electrical contact, thus causing pitting and erosion to the rail. In addition, arcing would cause an increase in resistance for the complete system and so would reduce the Laplace force. Accumulated pitting and erosion reduce the possibility of "good" electrical contact and cause arcing and wear, which shorten the life of the rails. The two main conditions for "good" electrical contact are the guarantee of a sufficient normal force from the contacts to the rails and a limitation of overheating of the contacts due to Joule effect.[31]

The threshold for a sufficient normal force to ensure good contact is referred to as Marshall's rule: 10 N/kA are required.[32] For our application, since the current is around 24 kA maximum, the corresponding contact force is around 240 N. In order to match this level of force, several sabot geometries were tested at low currents to select the most efficient geometry.

They are represented in Fig. 7. The first consists in wires of copper inserted into an armature of Delrin thermoplastic chosen for its rigidity, low-friction and low-deformability to shocks and its heat properties. It results in a mass of 40 g and is represented in Fig. 7(a). The second is a 170g X-shaped aluminum sabot with four feet having its extremities attached by an elastic band to ensure a return force, as can be seen in Fig. 7(b). The third consists in a bare plate of aluminum that is stuck between the two rails of 70 g and is represented in Fig. 7(c). Figure 8 shows the current waveforms measured during railgun shots for these three different geometries.

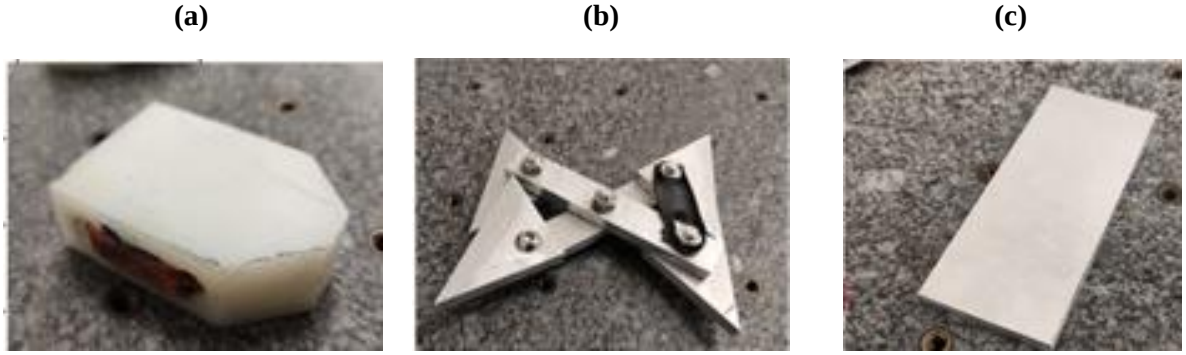

FIG. 7. Pictures of sabots: copper wires inserted into a Delrin armature (a), an X-shaped aluminum sabot (b) and a bare plate of aluminum (c).

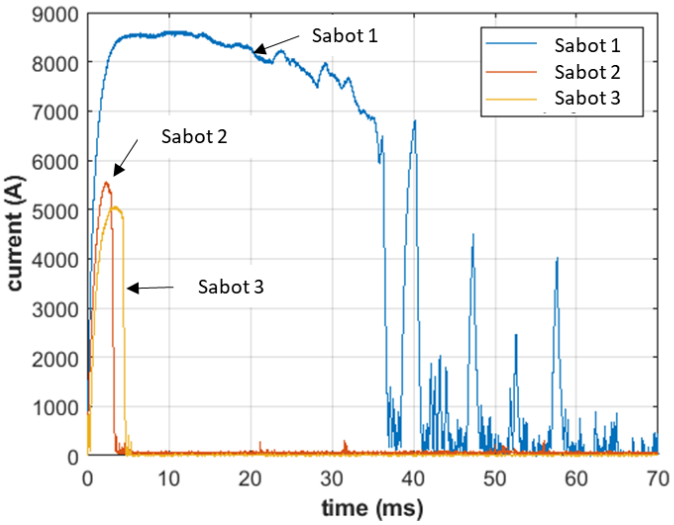

FIG. 8. Current waveforms of railgun shots for different sabots with an initial voltage of 12 V.

It can be observed that for the bare plate of aluminum and the X-shaped sabot, the current is initially established but is not maintained when the movement starts, whereas for sabot 1 the current reaches a higher level and is maintained continuously until electrical contact is lost at 37 ms. Even if peaks of current reappear after that moment, good contact is never again established and the sabot no longer gains consistent acceleration. Sabot 1 is believed to be able to maintain good contact during movement because its copper wire conductors, which are stuck between the Delrin armature and the rails, have enough spring tension to apply a sufficient normal force even if the wires are partially melted due to Joule effect and friction.

To avoid melting of the contacts, the dimensions of the copper wires have to be designed to endure heat load neglecting friction and constriction of the contacts.[33] Indeed, considering that the wires are only heated by Joule effect, an energy balance gives the required section of wire that is required to avoid melting:

$$S = \sqrt{\frac{\int I^2 dt}{\rho c \sigma \Delta T}} \tag{4}$$

where S is the section of the wires, I is the current, t is the time, ρ is the density, c is the heat capacity, σ is the electrical conductivity and ΔT is the temperature variation. Considering that the generator delivers a current of 24 kA during the predicted 100 ms and that the melting point of copper is 1085°C, the resulting minimum surface area is 14 mm^2.

This section has to be compared to the dimension of the skin effect, the expression of which for AC current is:

$$\delta = \sqrt{\frac{2}{\mu_0 \sigma \pi f}} \tag{5}$$

where δ is the dimension of the skin effect, μ_0 is the magnetic permeability of a vacuum, σ is the conductivity and f is the frequency. For square current waveforms between 50 ms and 100 ms, this dimension varies between 2 and 3 cm. Since the dimensions of the rail section are 22 mm wide and 12 mm high, the current is distributed over the whole section. Conventional railguns with timescales of less than 10 ms have a skin effect dimension of several mm so that the current flows in a small

section of the conductors and the wire inserted into the armatures that ensures contact and so causes its melting. However, the addition of several wires in parallel in the armature does not solve this problem by offering more conduction path. Indeed, for the insertion of several wires in parallel and a skin effect of less than 1 mm, most of the current flows through the back wire. This problem is referred to as velocity skin effect. [33, 34] In our case, the dimension of the skin effect is high enough due to a long duration of current injection so that the current is well distributed in the case of the insertion of several wires in the armature. This prevents the wires from melting due to Joule effect. For our application, wires composed of several hundred conductors with sections from 10 mm^2 to 15 mm^2 were inserted like a serpentine into the five holes of the Delrin armature to ensure three effective current paths, so that the thermal load for every wire is reduced by a factor of three.

The final Delrin thermoplastic armature consists in a rectangular block between 40 and 200 mm long depending on the selected length configuration, 47 mm wide and 12 mm high with five through holes in its side for inserting the conductor wires. The conductor wires have a total section of 10 mm^2. An image of a typical sabot consisting of the armature and wrapped copper wires is shown in Fig. 9. Figure 9(a) is an image of the sabot and Fig. 9(b) shows the insertion of the copper wire into the Delrin armature. The mass of the sabot can be varied between 45 to 210 g by changing the length of the Delrin armature and the length of the copper wire.

(a) **(b)**

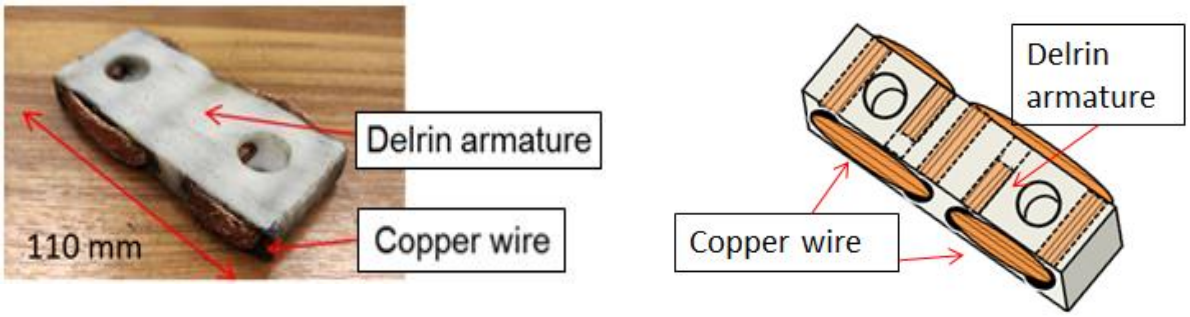

FIG. 9. Typical sabot composed of a Delrin armature and wrapped copper wires represented in a photograph (a) and in a diagram (b).

B. Evaluation of contact and rail resistance

As previously stated, the resistance of the railgun is a key parameter since 24 kA of current are expected with a 20 to 30 V setpoint from the capacitor bank. The circuit and the rail resistance during shot n°4 was measured by recording the voltage of the capacitor bank and the rails and the current in the circuit, as shown in Fig 10.

(a) **(b)**

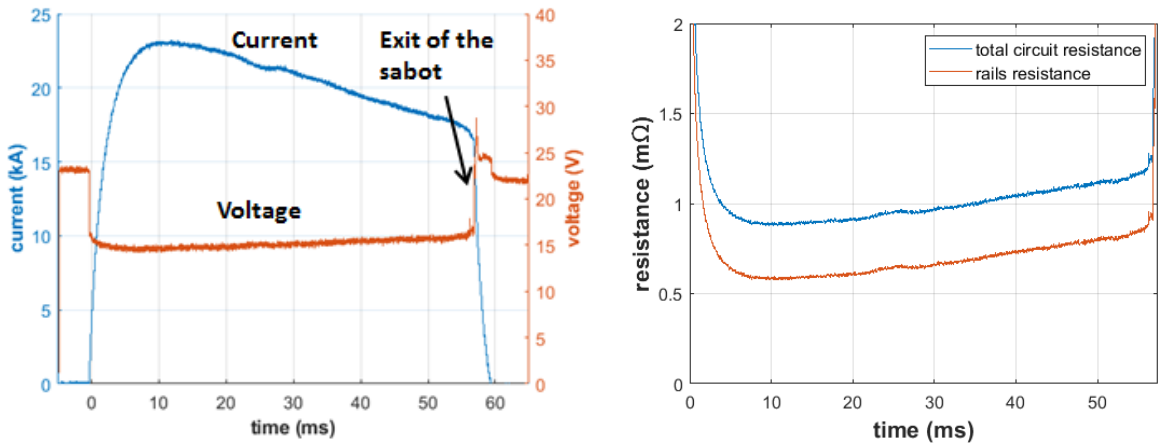

FIG. 10. Current and voltage waveforms at the terminals of the capacitor bank during shot n°4 (a) and resistance of the circuit and the rails (b).

The capacitor bank is initially charged to 24 V. At start time, the thyristor is activated, and the current increases in the circuit. The voltage measured at the terminals of the capacitor bank drops suddenly from 24 V to 16 V. This is due to the equivalent series resistance of the capacitor bank, which is around 0.29 mΩ: as the current reaches values up to 24 kA, it triggers a voltage drop of around 7 V so that the voltage of the circuit is considered to remain at 24 V during the shot. Indeed, a loss of only 1 V is measured after the shot. The electromotive force[35] also causes a drop of 1 to 1.5 V, which adds to the drop caused by the series resistance of the capacitor bank. As may be seen in Fig. 10(a), the current requires 10 ms to reach its maximum peak value of 24 kA due to the inductance of the circuit. This corresponds to the instant when the total resistance of the circuit reaches its minimum. After reaching its peak, the current drops from 24 kA to 17 kA in 46 ms almost linearly, the resistance of the circuit rises from 0.9 mΩ to 1.2 mΩ and the resistance in the rails rises from 0.6 mΩ to 0.9 mΩ, as can be measured in Fig. 10(b). This current drop is therefore explained by the additional rail portion leading to a final additional resistance of around 0.26 mΩ that fits the measurements. After 56 ms, the sabot exits the rails: the current suddenly drops to zero and the capacitor bank voltage returns to its initial value. It is interesting to note that, for this current magnitude, despite a longer current injection time compared to those of conventional railguns, the complex physical phenomena occurring at the contact point between the aluminum rails, the copper wires and the lubricant – Joule heating, the formation of a thin aluminum melt film, the ablation and wear of the rails[36] – do not have a noticeable impact on the current waveform at this initial contact force level.

C. Use of lubricant

To reduce friction during movement, the use of a hydrodynamic lubrication technique has been discussed over the last few years[37]. Even if, during movement, the melted layer of copper and aluminum that forms has a lubricant effect, the resulting erosion is able to cause a separation of the contact surfaces and degrade the current. The main investigations for a lubricant compatible with railgun technology have been carried for liquid lubricant, solid lubricant, and low-melting alloy lubricant.[37,38] Whereas liquid lubrication addresses experimental issues for the injection system and low-melting alloy lubrication requires an initial surface coating all along the rails, solid lubrication ensures ease of implementation, which enables fewer precautions to be taken. Despite Singer *et al.* [38] having reported that the use of PTFE reduces sabot contact surface wear in a configuration of copper rails with an aluminum sabot, thus reducing friction and ensuring a longer lifetime for the rails, this solution was found to be dangerous because the PTFE lubricant is highly flammable and is susceptible to start a fire with the melting contacts of the aluminum rails or the copper wires in the sabot. Thus,

the application of graphene grease was preferred and demonstrated a noticeable improvement in electrical contact during movement of the sabot, as can be seen in Fig. 11 when comparing shots n°3 and n°2.

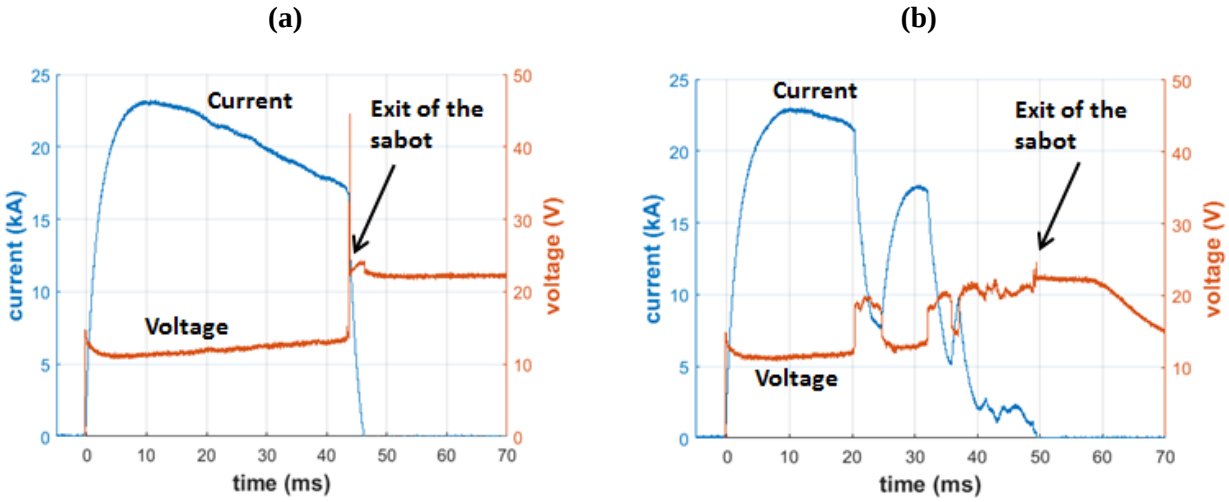

FIG. 11. Comparison of current and voltage waveforms at the rail terminals for shot n°3 with application of lubricant (a) and shot n°2 (b) without the application of lubricant.

In both Figs. 11(a) and 11(b) the peak current during the shot reaches a value of 23 kA, but whereas in Fig. 11(a) the current linearly drops to 18 kA at the exit of the sabot due to the reasons alluded to in Sec. III.B, in Fig. 11(b) a sudden drop of current from 22 to 7 kA in several ms appears at 20 ms and sparks are observed at the same time in the contact area between the sabot and the rails with the HSC. At this moment, the erosion of the rails after a few shots causes the concentration of the electrical contact in a shorter surface, focusing the Joule effect on these areas. Thus, the contact points from the copper wire in the sabot and from the rails start to melt, producing electric sparks. Evidence of this melting can be seen in Fig. 12, which shows a deposition of copper and erosion areas in the aluminum angles of the rails without use of lubricant. After this drop, the current intensity rises again as the electrical contact is re-established further on the rails but another drop of current occurs at 30 ms. This erosion is not only a problem because it brings about obsolescence of the rails but, since it reduces the current level, it reduces the electromagnetic force applied to the sabot, thus lowering its final speed. The use of a graphene lubricant helps to maintain the electrical contact during the crossing of the rails and so no drop in current occurs. This is at the same time a very efficient solution for the repetitiveness of the shots since the current waveforms from different shots then become very similar and lead to enhanced longevity of the aluminum angles covering the copper rails.

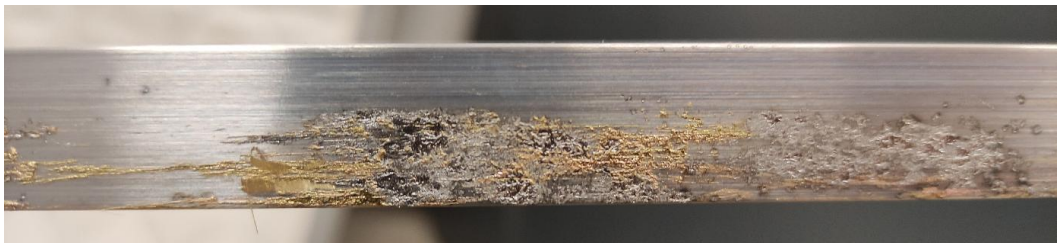

FIG. 12. Front view of an aluminum angle after several shots.

D. Overvoltage protection

A well-known problem with railguns is the formation of an electric arc when the sabot leaves the rails, triggered by the opening of the electrical circuit, as shown in Fig. 13. In Fig. 13(c), electric sparks coming from this arc can be observed.

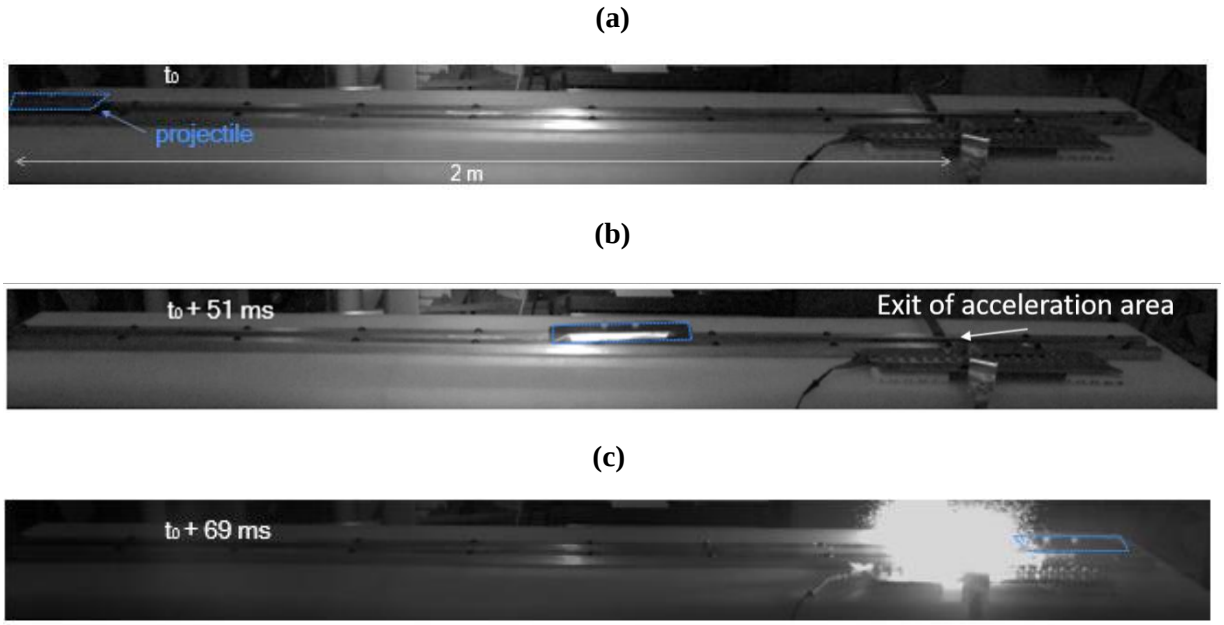

FIG. 13. Succession of images during a typical shot and appearance of an arc: (a) starting of the sabot, (b) acceleration, (c) exit and formation of a secondary arc.

If the electric arc only causes pitting and erosion damage to a relatively small area located at the very end of the rails, the current disruption represents a danger for the electrical components as represented in Fig 14 when comparing shots n°3 and n°4. Indeed, a rapid drop in current – around 20 kA in several ms - at the end of the rail imposes an overvoltage of up to 100 V, which propagates to the ultra-capacitor bank, as can be seen in Figs. 14(a) and 14(c) for shot n°3. This bank cannot withstand more than 34 V and protection is thus mandatory. 20 TVS model AK10-030C-Y diodes were used for this purpose. Figure 14(b) is a detail of Fig. 14(a) and Fig. 14(d) is a detail of Fig. 14(c) at the instants when the sabot exits the rails. As can be seen in Figs. 14(b) and 14(d) for shot n°4, when the current suddenly drops after the sabot's exit, they switch in less than one µs into a conducting state and damp the overvoltage at the terminals of the capacitor bank.

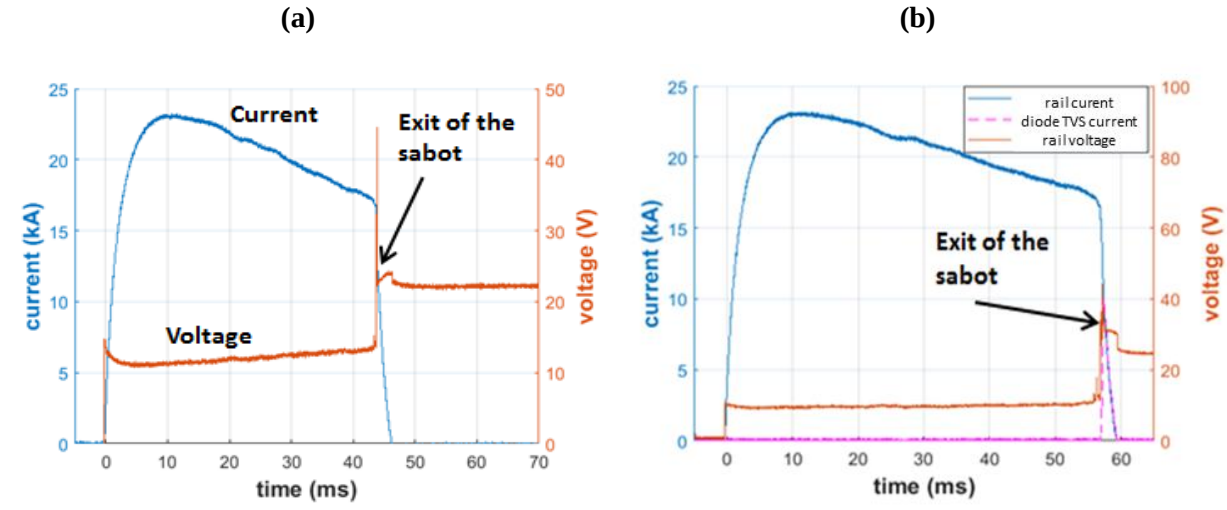

(c) **(d)**

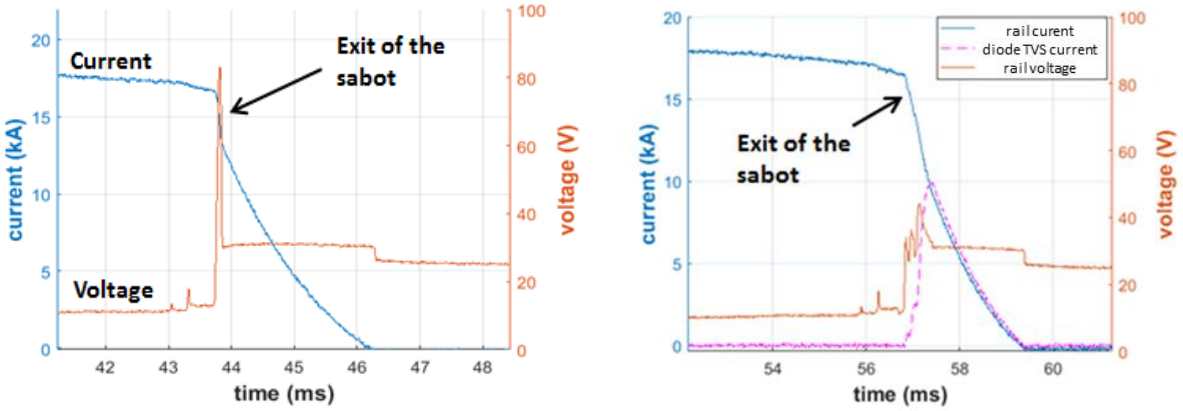

FIG. 14. Overvoltage measurement at the exit of the sabot (a) and (c) for shot n°3 and action of the TVS diodes (b) and (d) for shot n°4.

E. Eddy currents and de-magnetization

Interactions of the magnetic fields from the railgun and from the permanent magnets cause two side effects: the degradation of the propulsion efficiency by the creation of eddy currents and the demagnetization of the magnets with the railgun magnetic field.

The eddy currents are formed by the speed of the conductive sabot subjected to the permanent magnetic field. They are in opposition with the current circulating in the railgun so that they have to be removed to evaluate the real propulsion with the equivalent current. They can be evaluated using the formula:

$$I = \frac{Blv}{R} \tag{6}$$

with I being the eddy currents, B the magnetic density flux from the permanent magnets in the conductive wire, l the length of the conductive wire, v the velocity of the sabot and R the total resistance of the circuit. These currents are overestimated by introducing a velocity of 100 m/s, the magnetic density flux is around 0.3 H, the length of conductive wire in the sabot is 5 cm and the resistance of the circuit is around 1 mΩ. The resulting current is at the most 1500 A, which represents 6% of the maximum current and is consequently neglected in this study.

The de-magnetization of permanent magnets is more complicated to evaluate since the magnetic field induced by the railgun is orthoradial in the sabot referential. Thus, when the sabot passes over the magnets, its backward magnetic field is oriented in the same direction of the magnetic field induced by the permanent magnets and so contributes to their magnetization, whereas its rear field is oriented in the opposite direction and so demagnetizes them, as is represented in Fig. 15. Figure 15(a) represents a 3-D view of the augmented railgun whereas Fig. 15(b) represents a top-view of it.

(a)

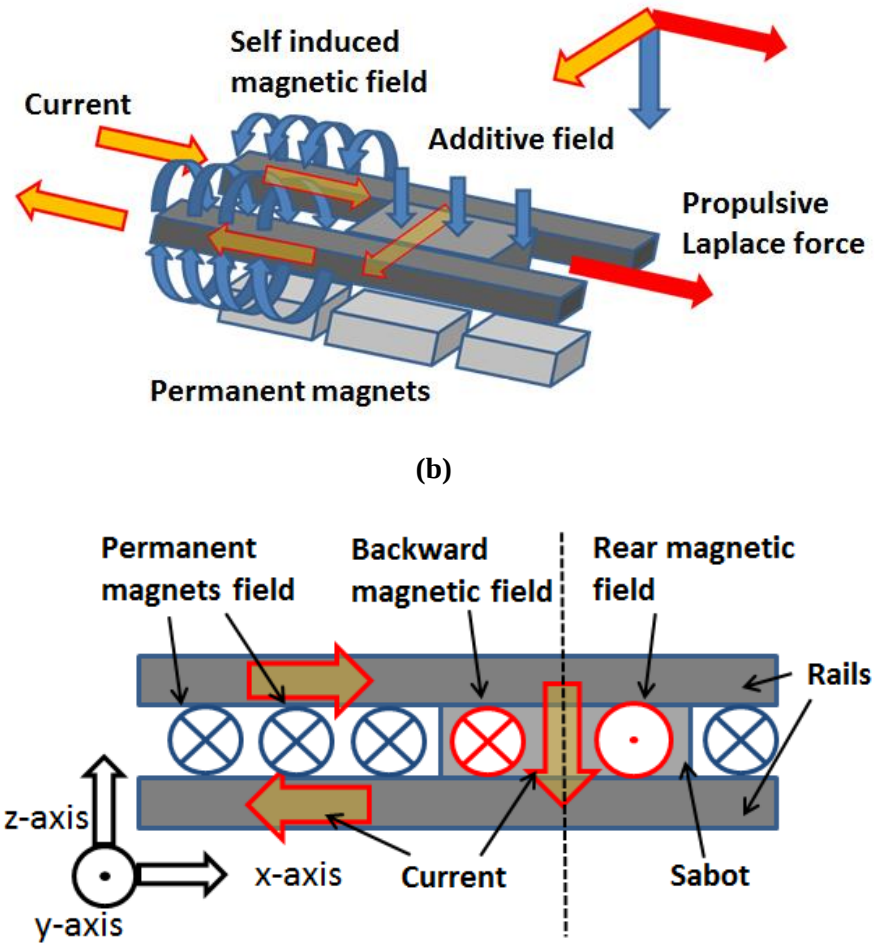

FIG. 15. 3-D diagram (a) and top-view (b) of magnetic fields produced by the railgun and by the augmented magnets.

Considering the expression of a magnetic field formed by the passage of current in an infinite wire in a plane perpendicular to the wire's direction, the projection of the magnetic field in the direction of the permanent magnet magnetic field, using Cartesian coordinates, is given by:

$$B = -sgn(x)\frac{\mu_0 I}{2\pi}\frac{x}{x^2+y^2} \tag{7}$$

where the origin of the coordinates is the wire, the x-axis is the axis of the sabot displacement; the y-axis is the axis perpendicular to the sabot displacement and parallel to the direction of the permanent magnet magnetic field. *Sgn* is the function sign, μ_0 is the magnetic permeability in a vacuum and I is the current that flows in the wire. This last expression is maximized when x equals y so that the maximum magnetic field for a given y-coordinate is:

$$B = -sgn(x)\frac{\mu_0 I}{4\pi y} \tag{8}$$

Since the surface of the magnets is situated at least 3 to 4 mm from the wire in our configuration, the evaluated field is at the most 800 mT and decreases to 260 mT in the centerline of the y-coordinate in the magnet. These fields are less than the specific flux of 1160 mT of these magnets so that they are

not de-magnetized by the magnetic field produced by the railgun. Moreover, this field is colinear to the direction of the magnet's field in the back of the sabot (x negative) and opposite to it in the rear of the sabot (x positive). Experimentally, no noticeable variation in the magnetic flux density was measured with a gaussmeter throughout the entire duration of the experiments.

IV. EXPERIMENTAL RESULTS AND COMPARISON TO THEORY

A. Ballistic analysis and evaluation of electromagnetic and friction forces

The performances of the developed railgun were analyzed by establishing the time varying displacement, speed and acceleration of the sabots during the different shots with different input parameters such as the mass of the sabot, the current waveform and the initial friction force. These ballistic curves were obtained using videos of the HSC and tracking software. Graphs of displacement and speed over time for shot n°4 are shown in Fig. 16.

To measure the displacement and the speed of the sabot, a 3 g plastic threated shaft was mounted on the sabot so that the tracking software could track the projectile made of the sabot and the threaded shaft. The HSC was positioned so that the railgun's length axis was recorded by the sensor over 1280 pixels. Thus, as 1280 pixels capture a length of 2.5 m, a pixel corresponds to 1.9 mm. Since the sampling rate is 20 kfps for a record of 100 ms, the uncertainty on the muzzle speed measurement is about 0.35 %.

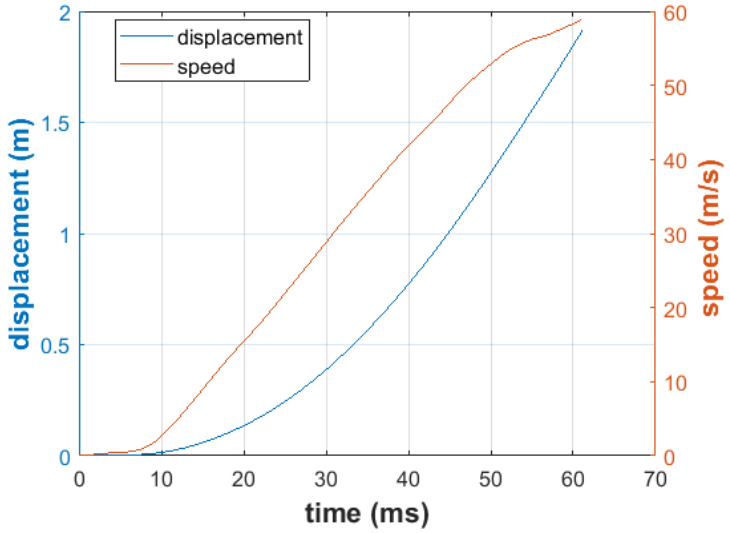

FIG. 16. Displacement and speed for shot n°4.

From these graphs, the acceleration of the sabot can be evaluated and the friction forces over time can be estimated using the fundamental principle of dynamics and Eqs. (1) and (3):

$$ma = \frac{1}{2}L'I^2 + BwI - F_f \tag{9}$$

where m is the mass and a the acceleration of the sabot. The two terms representing the electromagnetic force on the right side are evaluated by measuring the current waveform applied to the rails. F_f represents the friction force. Figure 17 shows the distribution of the different terms of Eq. (9) for shot n°1, the friction forces being evaluated with the difference of the other terms.

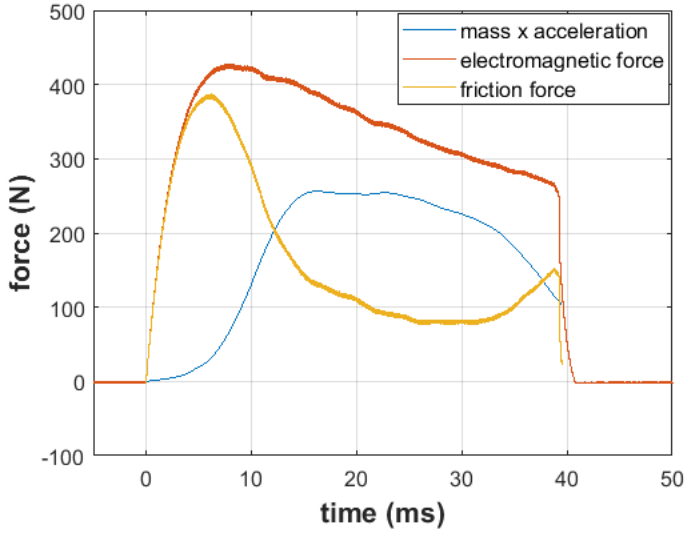

FIG. 17. Evolution of the terms of Eq. (9) during shot n°1.

As can be seen in Fig. 17, most of the electromagnetic force is lost in static friction at the first ms of the shot. Then, friction forces reach a peak before dropping in several ms, whereas the sabot acceleration increases and reaches a stable value of 250 N. This stable phase lasts around 25 ms before it starts to drop, when friction forces are again becoming dominant. Looking at the length of the rails, even if this ultimate boost of friction forces occurs in the last ms of the shot, it corresponds to a position in the middle of the rails. This suggests that this friction becomes important when the sabot has already reached a certain speed.

B. Evaluation of contact friction

Since good performances are possible only if a good electrical contact is ensured, friction forces cannot be neglected in a railgun application and represent the main loss of efficiency. The friction force is proportional to the normal force between the sabot and the rails. This normal force has a mechanical component due to the spring tension of the copper wires inserted between the rail and the armature and an electromagnetic component due to the bending of the copper wires at the contact surface with the rails that slightly diverts the electromagnetic propulsion force from the direction of the sabot displacement.[34,39] This electromagnetic component is proportional to the propulsion force and is expressed with an electromagnetic coefficient factor that varies between 10 to 50 % in the literature.[34,36,39] Thus, the expression of the friction force F_f is given by:

$$F_f = \mu\left(F_m + \gamma\frac{1}{2}L'I^2 + \gamma BwI\right) \tag{10}$$

where μ is the friction coefficient, F_m is the normal mechanical force and γ is the electromagnetic coefficient. Even if a model of dynamic friction coefficient as a function of velocity is presented in Gallant and Lehmann, [34] the dynamic friction coefficient is chosen constant since the range of velocities reached does not cause a dramatic drop in this coefficient. For a contact between copper and aluminum, the static coefficient is equal to 0.28, whereas the kinetic coefficient is equal to 0.23.[40] However, the use of a lubricant, as detailed in a further subsection, lowers this friction coefficient.

An estimation of F_m is possible using a simple model and a measurement of the initial resistance of the inserted sabot. Indeed, since a high normal contact force value is necessary to ensure good contact, this compression can be evaluated with a simple Holm model for *a-spots*. When current flows through a

contact surface, using a model of perfectly flat, circular, and isolated a-spots of radius a that concentrate current lines, Holm proposes a formula for the contact resistance[41]:

$$R_c = \frac{1}{2a\sigma} \tag{11}$$

where R_c is the contact resistance, a is the radius of an *a-spot* and σ is the conductivity of the material. As in the contact with aluminum rail and copper wire, the material with the smaller elastic modulus is aluminum; it will be the material causing the formation of the a-spots.

Since the resistance of the copper wire of 5 cm length and 30 mm^2 surface area is around 30 μΩ, the values from 200 to 600 μΩ measured as initial resistance before each shot are only due to the multiple contact points. This extent of initial resistance is obtained by slightly varying the section of the copper wires inserted in the Delrin armature between 10 and 15 mm^2. With this range of initial resistances, the dimension of an *a-spot* varies between 22 to 66 μm. Assuming elastic deformation, the relationship between the compressive force F_m and the surface of a-spots S is given by Hooke´s law:[42]

$$Fm = ES \tag{12}$$

where E is the elastic modulus of aluminum. The resulting mechanical force is between 100 and 1000 N and is estimated to remain constant during the sliding contact for most models even if the mechanical bending of the wires presumably changes with their partial fusion.[34]

In order to predict the performances of the railgun for different configurations, it is important to further analyze the dependence of the friction forces on the input parameters. The two friction force components are friction coming from the contacts and friction coming from air resistance.[39] Using the contact friction expression given in Eq. (10), Eq. (9) can be developed as follows:

$$ma = (1 - \mu\gamma)\left(\frac{1}{2}L'I^2 + BwI\right) - \frac{1}{2}C_D\rho_{air}Av^2 - \mu F_m \tag{13}$$

where C_D, ρ_{air}, and A are, respectively, the coefficient of windward resistance, the air density, and the windward area. In the case of a square shaped windward area, the coefficient C_D is around 1. It is assumed in Gallant and Lehmann[34] and in Schneider *et al.*[36] that the factor γ represents the proportion of copper wires that is bent due to contact with rails compared to the total length of the wires in the sabot. As Gallant and Lehmann [34] report a γ value of 0.154 for copper wires and an inter-rail distance of 15mm, it is expected that the factor γ is even lower for our copper wires and inter-rail distance of 50mm. Moreover, since the coefficient of dynamic friction μ between copper and aluminum is estimated to be less than 0.3, the factor μ times γ in Eq. (13) is less than 0.05 and is thus neglected in the remainder of the analysis.

In addition, as seen in Sec. III.C, after the current applied to the rails has reached its maximum peak – this delay being due to the parasitic inductive behavior of the circuit – the evolution of the current can be correlated to the longer part of the rails crossed by the current during the shot. Thus, an expression of the current depending on the displacement of the sabot can be found. Indeed, since the rail voltage is constant during the shot, as shown in Fig. 10, the expression of the current over displacement can be written as:

$$I(l) = I_{peak}\frac{R_0}{R_0 + rl} \tag{14}$$

where R_0 is the initial resistance of the circuit, r is the linear resistance of the rails and l is the displacement of the sabot. Fig. 18 shows a comparison between the current waveform of shot n°4 and the plot of expression 14 with R_0 being 0.9 mΩ and r being 0.26 mΩ/m and using the ballistic curves of the shot. It can be seen that beside the initial part where the current increases due to the circuit inductance, the current drops at the same rate as the theoretical expression.

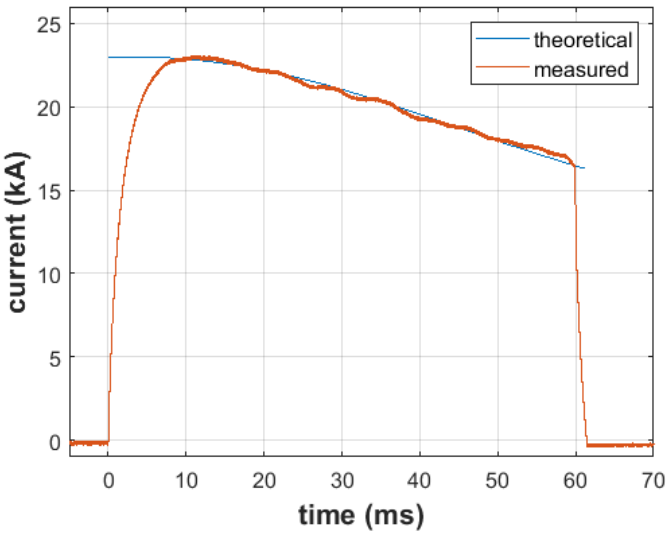

FIG. 18. Comparison of theoretical and measured currents in the railgun for shot n°4.

Thus, if we replace equation (14) in equation (13), the latter becomes a non-linear differential equation:

$$m\frac{d^2l}{dt^2} = \frac{1}{2}L'I_{peak}^2\left(\frac{1}{1+\left(\frac{r}{R_0}\right)l}\right)^2 + BwI_{peak}\frac{1}{1+\left(\frac{r}{R_0}\right)l} - \frac{1}{2}C_D\rho_{air}A\left(\frac{dl}{dt}\right)^2 - \mu F_m \tag{15}$$

with the limitation that it can be applied only after the sabot starts to move due the hypothesis in equation 14 and with the factor μ being set as the dynamic friction. In all the shots, it was observed that the sabot started to move before the current reached its peak so that the second condition is the limiting condition. From this equation, it is interesting to deduce the dynamic friction coefficient to complete the model and then predict the performances of the circuit for different configurations.

To obtain an estimation of μ, shots n°1, n°3 and n°4, which have varying parameters of mass, input current and initial transverse mechanical force F_m, were successfully analyzed. Their displacement, speed, acceleration and current waveform were recorded and the factor μ was determined by fitting the measured displacement and the calculated displacement resulting from the solving of the differential Eq. (15) using a least-squares procedure. An example of adjustment is represented in Fig. (19) for shot n°1. Table II summarizes the results of the analyzed shots.

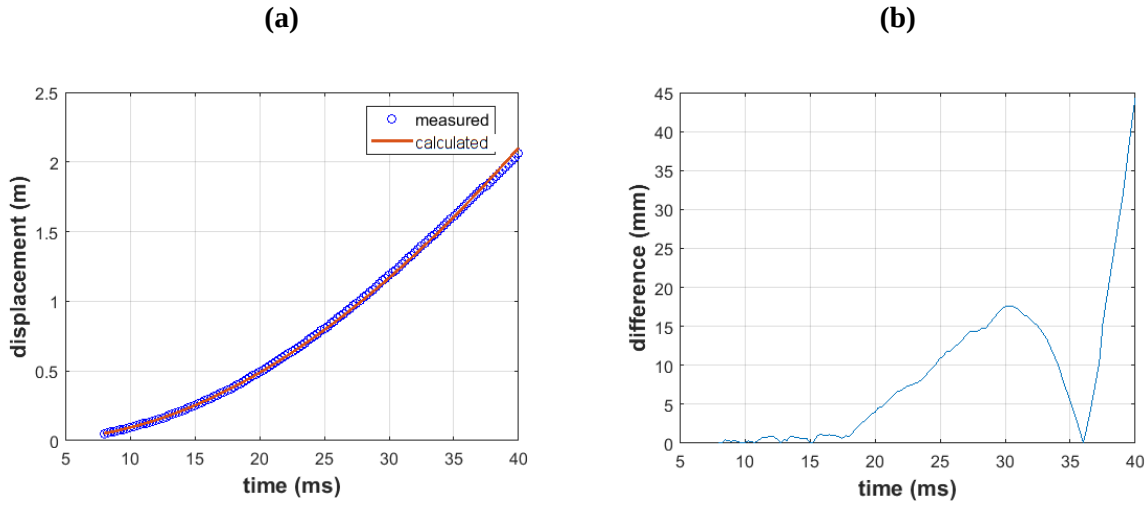

FIG. 19. (a) Fitting of a measured curve using a least-squares procedure to calculate the friction forces for shot n°1 and (b) absolute difference between the measured and calculated values over time.

TABLE II. Analysis of the different shots.

Shot n°	Initial contact resistance (μΩ)	Initial mechanical force F_m (N)	Start of motion after trigger (ms)	μ	μ F_m (N)
1	280	486	5	0.307	149
3	540	136	2	1.165	158
4	230	748	10	0.1895	142

In Table II, the initial mechanical force is calculated using Eqs. (11) and (12). The coefficient μ is the fit parameter when comparing the calculated and measured displacement. Despite the fact that the coefficient of dynamic friction was expected to be constant for the three shots, it turned out it was able to vary from less than 0.2 to more than 1, which is physically impossible. A possible interpretation is that the mechanical force is uncorrelated with the friction force after motion has started. Indeed, the resulting average friction force μF_m appears to be a constant quantity in the three shots, even though the initial mechanical forces have a difference of a factor up to 5 between shots 3 and 4. Thus, a model of a constant friction force not dependent on the initial mechanical force seems more relevant for our railgun facility.

However, the initial mechanical force does have an influence on the instant of motion after the insertion of the current: a high initial mechanical force delays the instant of motion. Indeed, the current

in the rails has to exceed a threshold value so that the electromagnetic force becomes high enough to overcome a given level of static friction forces and thus the moment of initial motion depends on the current rise time to reach this threshold. If the initial mechanical force exceeds a certain threshold, the electromagnetic force will not be enough to overcome the static friction forces at the peak of the current and motion will never occur. Moreover, if the initial mechanical force is too low, a good electrical contact cannot be ensured and the current in the rails is likely to drop dramatically during the shot (see Sec. III A). Indeed, for initial resistances over 600 μΩ, and initial mechanical forces below 100 N, the recorded shots never exhibited a stable current waveform. It can be noted that Marshall's rule, evoked in Sec. III.A, which predicts that a 240 N mechanical force is required to ensure good electrical contact for 24 kA of current injection, is not always respected in our case since shots with an initial mechanical force between 130 and 240 N were successfully carried out. To explain this behavior, we can mention that Holm's formula and Marshall's rule are an approximation and that good electrical contact for shots between 100 and 300 N of initial mechanical force was not always ensured during the shot.

After this initial motion phase, the initial mechanical force does not influence the displacement of the sabot and a model of constant friction force due to the rails is able to describe the experimental results.

C. Performances achieved by the railgun

The experimental performances of the developed railgun in terms of speed, acceleration and kinetic energy for various parameters, namely voltage, peak current and mass are listed in Table III.

TABLE III. Experimental performances of the railgun.

Shot n°	Mass(g)	Voltage (V)	Current peak (kA)	Muzzle velocity (m/s)	Mean acceleration (m/s^2)	Kinetic energy (J)
5	45	25	22	125	7810	351
6	100	25	24	100	5000	500
7	150	25	24	80	3200	480
8	175	25	24	77	2960	518
9	210	25	24	66	2180	457

The results of this table show that sabots from 100 to 200 g can be propelled to a speed of between 66 and 100 m/s – the limiting factor being the maximum peak current acceptable for the capacitor bank. This speed range is of the same order of magnitude of the speed of an aircraft when the risk of lightning strike is most likely – at take-off or landing phases – so that the use of this railgun facility is relevant to the problematic of the gliding arc even if the values are in the lower range of the phenomenon.

D. Evaluation of standard deviation

In order to determine the repeatability of the shots and thus the acceptability of the instrument as a launcher for lightning experiments, a study of the standard deviation for a series of shots with different experimental conditions was conducted. Three series of shots were carried out, varying the mass of the sabot and the current peak injected. The results of the muzzle velocities obtained, their standard deviations and their comparison to theoretical values are shown in Table IV. The theoretical values are obtained solving Eq. (15) with the factor μF_m being constant and equal to 150 N in adequacy with the analysis conducted in Sec IV.B.

TABLE IV. Evaluation of standard deviation.

Number of shots	Mass (g)	Mass standard deviation (g)	Current peak (kA)	Current peak standard deviation (kA)	Muzzle velocity (m/s)	Muzzle velocity standard deviation (m/s)	Theoretical muzzle velocity (m/s)	Difference (%)
13	194.4	3.0	22.4	0.7	51.9	2.9	55.9	7.1
4	191.3	2.5	19.8	0.5	41.5	2.4	46.2	10.2
4	373.8	2.5	22.3	0.5	38.9	4.1	40.0	2.8

The first row of Table IV shows that 13 shots with similar initial conditions were performed successfully with a standard deviation of 5.6% at a mean velocity of 51.9 m/s, which proves the relatively good repeatability of the instrument to study aircraft lightning strikes. However, Siaenen *et al*.[43] achieved a muzzle velocity statistical deviation of 1.63% at a mean velocity of 285 m/s without control. Thus, a standard deviation of 5.6% is not exceptional for this application.

The theoretical muzzle velocity has a maximum difference of 10.2% with the experimental muzzle velocities. This difference can be inferred to the simple model of a constant friction force during the shots. Moreover, the use of Eq. (14) in the force model amounts to neglecting the initial current rise phase due to the circuit's inductance and thus to overestimating the Laplace force in the first instants of the shot.

V. EXPERIMENTAL COUPLING OF THE RAILGUN TECHNOLOGY AND A LIGHTNING ELECTRIC ARC FACILITY

To reproduce the sweeping of a lightning arc, two electrodes of an electrical generator were positioned just after the extremity of the rails so that the aircraft test plate was hit by the electric arc when the current of the railgun no longer flowed in the copper wires of the sabot. This precaution was taken to prevent the high voltage of the arc generator from discharging through the railgun electrical circuit. A receptacle consisting in a sand filled wooden box to stop the projectile was placed 1 m after the electrodes. Three types of electrode were tested: a bare rod of tungsten, a rod of tungsten protected by a diverter at its extremity to avoid the influence of the electrode shape, and a plate of aluminum. Figure 19 presents the configuration of the electrodes where the electrode above is a rod of tungsten of 10 cm diameter with a dielectric diverter ball at the tip, and the electrode below is an aluminum plate. Figures 20(a) and 20(b) are respectively a picture and a schematic diagram of the configuration set-up.

(a)

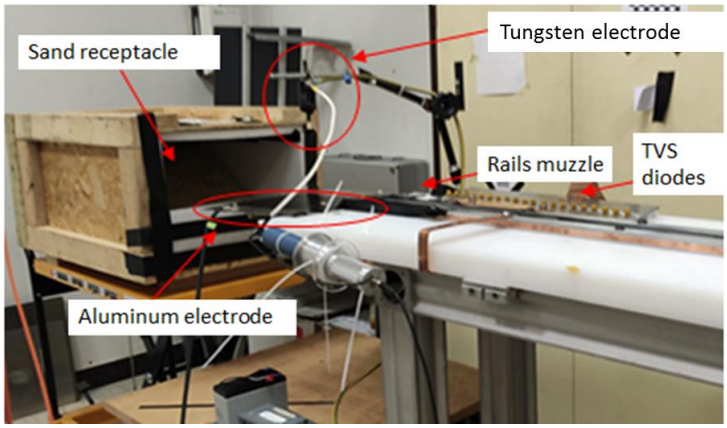

(b)

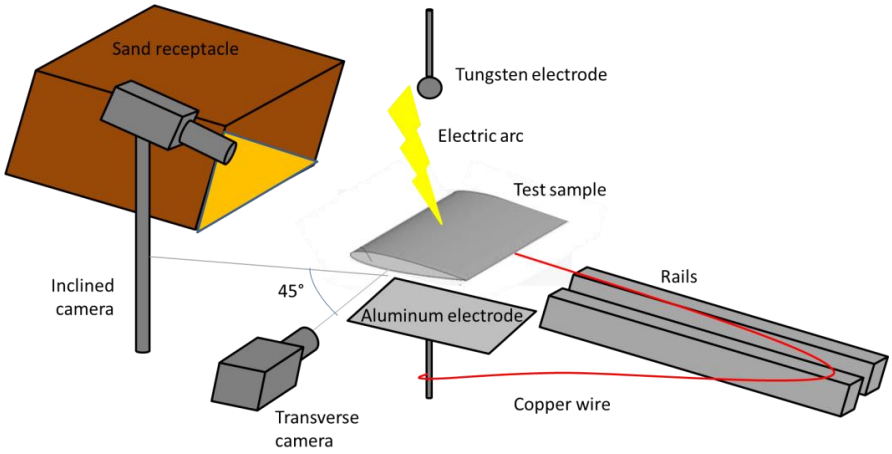

FIG. 20. Photo (a) and schematic diagram (b) of the electrode's configuration at the exit of the railgun facility.

The lightning generator is able to reproduce a C*-lightning waveform electric arc as recommended by the lightning standard (ARP5412A 2013):[44] The generator produces an electric arc that can be extended to more than 1 m with a current shape of 400 A ± 10% during 100 ms.[45] The initial distance between both electrodes is set at 50 cm and centered in the projectile axis so that the plasma jets in the vicinity of the electrodes do not affect the interaction of the electric arc and the test plate during the lightning strike. Since, during the strike, the electric arc is able to be elongated to more than 1 m, the inter-electrode electric potential can reach up to 2 kV. Thus, great attention is required to ensure the

electric isolation between the lightning electric arc and the electrical circuit of the railgun is limited to 25 V.

To synchronize the lightning strike with the arrival of the projectile, the lightning arc is initiated 20 ms before the estimated time of arrival, based on the velocity value of the projectile obtained in Table I. The ignition of the electric arc is done using a thin conductive copper wire that vaporizes by Joule effect when the current rises. This rapidly heats the surrounding air and contributes to generating high-density plasma.[46] The 20 ms margin gives enough time for the electric arc to achieve a stable column shape.

In order to analyze the influence of the air flow profile on the sweeping phenomenon and to be more relevant with the aeronautical context, the shape of the aircraft material for the coupling with lightning was changed from a plate to a NACA 0012 airfoil. The test material – a foil of aluminum with 0.4 mm thickness is modelled in respect to the NACA airfoil and juts out of the sabot using two plastic rods, as presented in Fig 21. The sabot has a mass of 80 g and the payload has a mass between 100 g and 150 g.

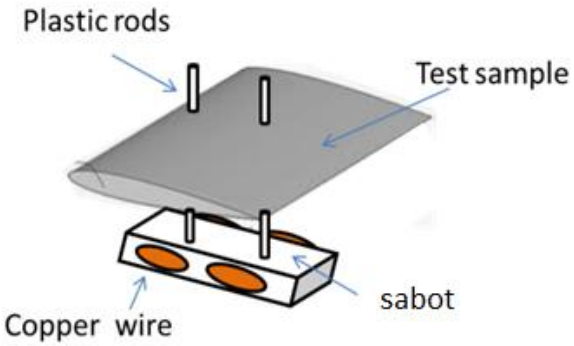

FIG. 21. Diagram of a projectile composed of the test sample and the sabot.

For this application, since the payload is screwed on the dead mass, there is no separation of the two elements after the muzzle exit, as usually happens for railgun applications. Figure 22 shows a succession of images recorded by HSC of a lightning strike on this NACA shape.

(a) **(b)**

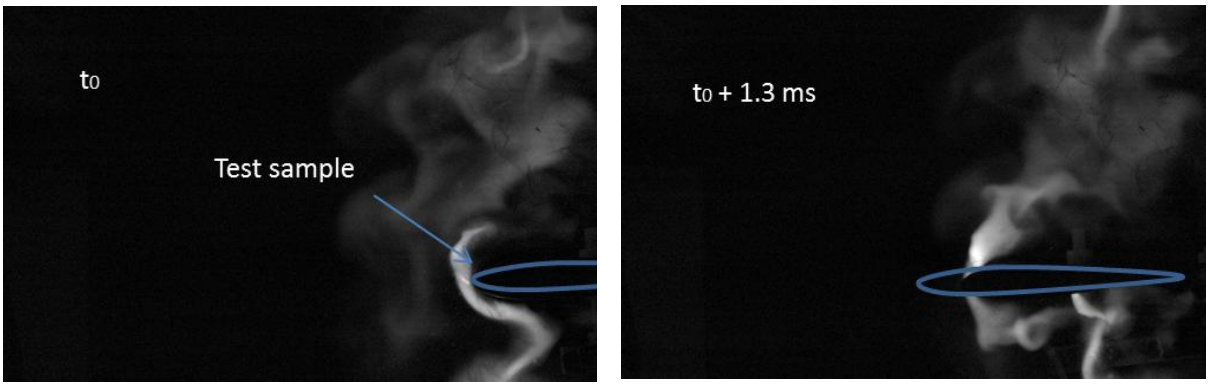

(c) **(d)**

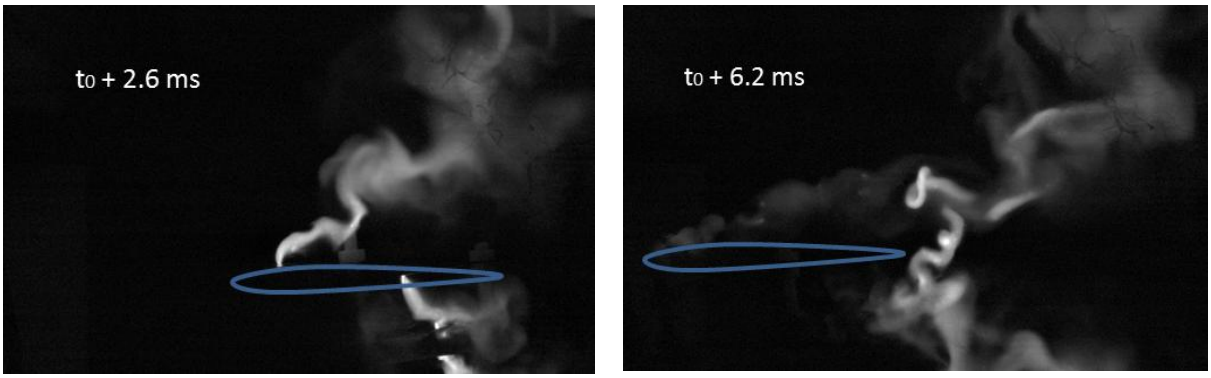

FIG. 22. Succession of images of a projectile crossing an electric arc with a cathodic arc root above and an anodic arc root below. (a) t_0, (b) t_0 + 1.3 ms, (c) t_0 + 2.6 ms and (d) t_0 + 6.2 ms.

In Fig. 22(a), the arc channel is already formed between two electrodes consisting of two tungsten rods with a diverter and the material test sample is pushing the electric arcs. In Fig. 22(b) the sample has divided the arc column into two smaller arc columns, thus forming two arc roots on its surface so that the lightning current flows from the cathodic root to the anodic root through the aluminum sample. During movement of the sample, the two columns formed are elongated and the arc roots either stick, have a continuous sweeping movement, or leap onto the material test surface. After the passage of the sample, the lightning channel can either reform from the two column channels or extinguish. However, it is preferable to study only one arc root to avoid any coupling in the displacement of the two arc roots along the material test sample. This situation is more relevant for the study of aircraft lightning strikes since the two arc roots are not displaced on surfaces belonging to the same pieces in a real case and thus it is complicated to know the current path in the aircraft structure. To bypass this difficulty, a copper wire with a section of 0.15 mm^2 and a length of 3 m was screwed onto the lower surface of the material test sample. This wire was extended before the shot and the other extremity was screwed onto the lower electrode of the lightning generator, near the exit of the railgun facility. This also had the advantage that the lightning arc only glided on the upper area of the test sample and thus the sabot did not influence the phenomenon. Figure 23 shows a succession of images of a shot with the displacement of the copper wire.

(a)

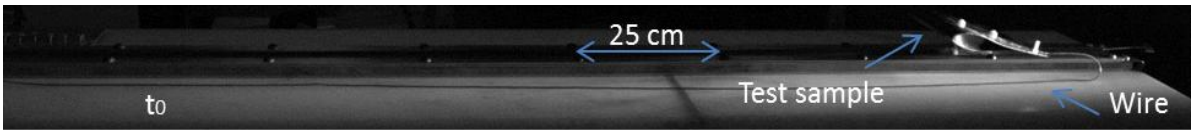

(b)

(c)

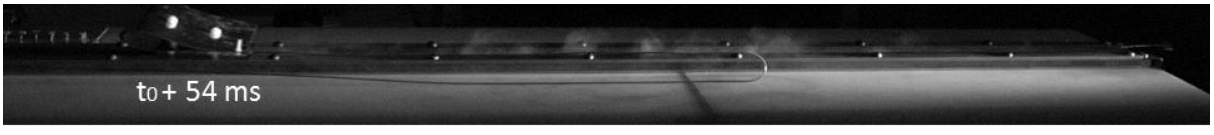

FIG. 23. Succession of images of a shot of a test sample connected to a wire. (a) t_0, (b) t_0 + 32 ms and (c) t_0 + 54 ms.

It may be seen that the acceleration of the projectile is so important that it moves faster than the propagation of the elongation wave in the wire: indeed, we can observe that the projectile moves faster than the bend of the wire. Fig. 24 shows a succession of different images of the interaction of a test sample crossing an electric arc, the test sample being connected to the underlying electrode with a copper wire.

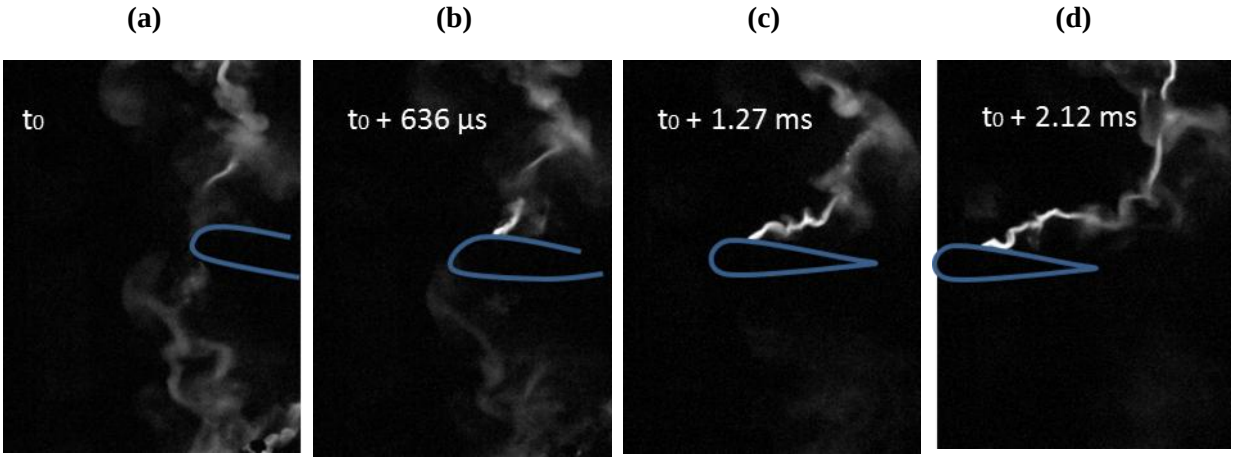

FIG. 24. Succession of images of a test sample crossing an electric arc with a cathodic arc root above and a copper wire beneath. (a) t_0, (b) t_0 + 636 µs, (c) t_0 + 1.27 ms and (d) t_0 + 2.12 ms.

In Fig. 24(a), the arc channel is already formed between two electrodes consisting of two tungsten rods with a diverter and the material test sample is pushing the electric arcs. In Fig. 24(b) the sample has crossed the arc column: only the part of the electrical channel above the sample has remained, forming an arc root on its surface, whereas the lower part starts to fade away because the current flows through the copper wire to reach the ground. Indeed, the copper wire is less resistive than the electric arc – 90 mΩ for the copper wire compared to around 0.5 to 1 Ω for 25 cm of a 400 A electric arc.[45] In Figs. 24(c) and 24(d) the electric arc is elongating, and the arc root is sticking onto the test sample. Since the electric arc channel cannot reconnect to the other electrode by bypassing the current branch in the copper wire, it is extended until it reaches a length above 1 m, causing its extinction because the lightning generator cannot provide enough voltage to sustain the arc. Therefore, this configuration of projectile shot with a copper wire connected to an electrode of the lightning generator has proved relevant for studying the motion of a single arc root during a lightning strike. However, the addition of a wire that is pulled during the experiment reduces the speed reached by the test sample. Indeed, whereas a projectile of 150 g is able to reach 70 m/s, it dropped to 55 m/s using the wire.

With this configuration an experimental campaign of about fifty shots was successfully conducted. The main advantage of the developed low voltage railgun is that the security process is less restrictive than for a conventional railgun and the supply voltage is not drained out after one shot. Thus, only 5 to 10 minutes are required between two shots to record the videos of the HSC, to change the entire projectile, to check the condition of the rails and to renew the lubricant.

VI. CONCLUSIONS

An experimental implementation of an unconventional railgun capable of launching test samples of several hundreds of grams at speeds up to 100 m/s with an initial voltage of around 20 V was carried out to study the interaction between a sweeping electric arc representative of the lightning C* waveform and an aeronautical aluminum test sample.

Since an initial overview of the linear propulsion means showed that electromagnetic launchers are a relevant solution in terms of acceleration performances and safety issues, a railgun electrical circuit was designed: this circuit differs from conventional railgun electrical circuits since it involves high capacitance, low voltage capacitors, also referred to as ultra-capacitors in the literature. It has the direct advantage of performing a launch with an operating voltage of only 20 V, which makes it safe to use since it is meant to be coupled with a high-power lightning facility. The current generator developed in this work consists of 144 of these ultra-capacitors for an equivalent capacitance of 3000 F and is able to inject a peak current of 24 kA over several tens of ms into the rails.

With this electrical configuration, the experimental implementation of a railgun was conducted. The low operating voltage and the requirement of good sliding contact time duration of several tens of ms raise experimental issues that have not been discussed before in the literature. The different problematic aspects are the maintenance of a good electrical contact through the study of mechanical friction and the electric resistances of the circuit. The addition of permanent magnets providing a supplementary magnetic field of 300 mT and the problems of overvoltage are also discussed.

Once these technical problems had been addressed, railgun shots were operated for different initial conditions such as the payload of the projectile, the initial friction force and the peak current in order to perform ballistic studies. A model of friction forces during the shot was then developed analyzing the motion of the projectile and establishing a force balance. The model shows that a constant friction force can be assessed to fit the data after the projectile has started to move and it is interesting to predict the performances of shots varying the initial conditions. Then, projectiles from 100 to 200 g were propelled to speeds between 66 and 100 m/s, which is below the high range requirements of the objective: propel a projectile of 500 g at 100 m/s, but this is still of the same order of magnitude as the speed of an aircraft when the risk of lightning strike is most probable – at take-off or landing phases, the developed railgun proved relevant to the study of the swept stroke phenomenon.

The railgun facility was finally coupled with a lightning arc generator facility and the first swept stroke images using this test bench are presented. For future work, we expect to conduct an ambitious campaign to study the swept stroke in detail for many different configurations and to establish a relevant database of the physical parameters of the phenomenon.

ACKNOWLEDGMENTS

The authors would like to thank the French Civil Aviation Authority (DGAC) for its support. As well as Stanley O. Starr (NASA), Robert C. Youngquist (NASA), Philippe Delmote (ISL) and Markus Schneider (ISL) for their precious experimental advice.

DATA AVAILABILITY

The data that support the findings of this study are available from the corresponding author upon reasonable request.

REFERENCES

[1]J. A. Plumer, *in Int. Conf. on Lightning Protection, Vienna* (2012).

[2]A. Larsson, P. Lalande, A. Bondiou-Clergerie and A. Delannoy, *J. Phys. D: Appl. Phys.* **33** 1866 (2000).

[3]C Guerra-Garcia, N. C. Nguyen, J. Peraire and M. Martinez-Sanchez, *J. Phys. D: Appl. Phys.* Phys. **49** 375204. (2016).

[4]F. Tholin, L. Chemartin and P. Lalande, *in Int. Conf. on Lightning and Static Electricity, Toulouse* (2015).

[5]K. Koyama, H. Toya, Y. Wasa and A. Hasegawa, in IEEE Trans. Magn. vol. 29, no. 1. (1993)

[6]A. E. Guile and P. E. Secker, J. Appl. Phys **29**, 1662-1667 (1958).

[7]P. R. Zeller and W. F. Rieder, in *IEEE Transactions on Components and Packaging Technologies*, vol. 24, no. 3, (2001).

[8]D. W. Clifford and L. E. McCrary. Final report: simulated lightning test Shuttle .03 scale model. Report number MDC A3155, (1974).

[9]L. L. Oh, and S. D. Schneider, *in Int. Conf. on Lightning and Static Electricity, Abingdon* (1975).

[10]J. A. Dobbing and A. W. Hanson, *in 1978 International Symposium on Electromagnetic compatibility*, Atlanta (1978).

[11]R. Vermorel, N. Vandenberghe and E. Villermaux, Proc. R. Soc. A **463**, 641–658 (2007).

[12]E. Huggins, The Physics Teacher **46**, 142 (2008).

[13]C. Ross. Mechanics of Solids, *Elsevier Science* (1999).

[14]D. Keeports , The Physics Teacher **34**, 460-461 (1996)

[15]H. B. Ahmed, B. Multon, N. Bernard and C. Kerzreho *La Revue 3 E. I, Société de l'électricité, de l'électronique et des technologies de l'information et de la communication*, 18-29. (2007).

[16]N. Pilz, H. Adirim, R. Lo and A. Schildknecht, *in Proc. 2nd Int. Conf. on Green Propellants for Space Propulsion*, Sardinia (2004).

[17]D. B. Longcope, Int. J. Impact Eng. Vol. 17, 4-6 (1995).

[18]A. Cassat, N. Corsi, R. Moser, N. Wavre, in 4th Int. Symp. on Linear Drives for Industry Application, Birmingham (2003).

[19]H. D. Fair, *IEEE* Trans. Magn. vol. 33, no. 1 (1997).

[20]I. R. McNab, *IEEE* Trans. Magn. vol. 39, no. 1 (2003).

[21]H. D. Fair, *IEEE* Trans. Magn. vol. 29, no. 1 (1993).

[22]H. Tamura and A. B. Sawaoka, Rev. Sci. Instrum. 63, 3102-3107 (1992).

[23]J. V. Parker, in *IEEE* Trans. Magn. vol. 25, no. 1, pp. 418-424 (1989).

[24] P. Lehmann, H. Peter and J. Wey, in *IEEE* Trans. Magn. vol. 37, no. 1 (2001).

[25]S. C. Rashleigh and R. A. Marshall , J. Appl. Phys. **49**, 2540-2542 (1978).

[25]L. Dai, Q. Zhang, H. Zhong, F. Lin, H. Li, Y. Wang, C. Su, Q. Huang and X. Chen, Rev. Sci. Instrum.86, 074703 (2015).

[26]J. V. Parker, J. Appl. Phys. **53**, 6710-6723 (1982).

[27]P. Sharma and T. S. Bhatti, Energy Convers. Manag. Vol 51, Issue 12, 2901-2912 (2010).

[28]Stanley O. Starr *and* Robert C. Youngquist, Am. J. Phys. **81**, 38-43 (2013).

[29]L.J Giacoletto, Electronic Designer's Handbook, McGraw-Hill Book Company (1977).

[30]S. Katsuki, H. Akiyama, N. Eguchi, T. Sueda, M. Soejima and S. Maeda, Rev. Sci. Instrum**. 66** 4227-4232 (1995).

[31]M. Schneider, D. Eckenfels and F. Hatterer, in *IEEE Trans. Magn*. vol. 39, no. 1, pp. 76-81, (2003).

[32]J. P. Barber, D. P. Bauer, K. Jamison, J. V. Parker, F. Stefani and A. Zielinski, in *IEEE Trans. Magn*. vol. 39, no. 1, pp. 47-51, (2003).

[33]J. P. Barber and A. Challita, in *IEEE Trans. Magn*. vol. 29, no. 1, pp. 733-738, (1993).

[34]J. Gallant and P. Lehmann, in *IEEE Trans. Magn*. vol. 41, no. 1, pp. 188-193, (2005).

[35]I.R. McNab, *in IEEE Trans. Magn*. vol.39, no.1. pp. 498–500. (2003).

[36]M. Schneider, D. Eckenfels and S. Nezirevic, in *IEEE Trans. Magn*. vol. 39, no. 1, pp. 183-187 (2003).

[37]J. Chen and Q. Lv IOP *Conf. Ser.: Earth Environ. Sci.* **170** 042089 (2018).

[38]I. L. Singer, M. J. Veracka, C. N. Boyer and J. M. Neri, in *IEEE Trans. Magn*. vol. 39, no. 1, pp. 138-143 (2011).

[39]C. Zhu, B. Li, Defence Technology, Volume 16, Issue 4, Pages 747-752, (2020).

[40]P. J. Blau, ASM Handbook, vol 18, Friction, Lubrification and Wear (1992).

[41] R. Holm. Electric Contacts: Theory and Application, (1967).

[42] M. Braunovic, N. K. Myshkin, V. V. Konchits, CRC Press, Electrical Contacts: Fundamentals, Applications and Technology (2017)

[43] T. Siaenen, M. G. Schneider, and M. J. Löffler in *IEEE Trans. Plasma Sci*., vol. 39, no. 1, pp. 133–137 (2011).

[44]SAE ARP5412B and Eurocae ED-105A, *Aircraft Lightning Environment and Related Test Waveforms* (AE-2 Lightning Committee, SAE International, London 2013).

[45]V. Andraud, R. Sousa Martins, C. Zaepffel, R. Landfried and P. Testé, Rev. Sci. Instrum**. 92**, 104709 (2021).

[46]A. Kadivar, K. Niayesh, N. Støa-Aanensen and F. Abid, J. Phys. D: Appl. Phys. **54** 055203. (2020).